GEOLOGY | THE GEOLOGICAL SOCIETY OF AMERICA®

https://doi.org/10.1130/G46107.1

Manuscript received 7 February 2019
Revised manuscript received 2 April 2019
Manuscript accepted 10 April 2019

Published online 2 May 2019

Change in seismic attenuation as a long-term precursor of gas-driven eruptions

Corentin Caudron[1], Társilo Girona[2], Benoît Taisne[3,4], Suparjan[5], Hendra Gunawan[5], Kristianto[5], and Kasbani[5]
[1]Université Grenoble Alpes, Université Savoie Mont Blanc, CNRS, IRD,IFSTTAR, ISTerre, 38000 Grenoble, France
[2]Jet Propulsion Laboratory, California Institute of Technology, Pasadena, California 91109, USA
[3]Earth Observatory of Singapore, 639798 Singapore
[4]Asian School of the Environment, 639798 Singapore
[5]Center for Volcanology and Geological Hazard Mitigation, Bandung 40122, Indonesia

ABSTRACT

A large fraction of volcanic eruptions do not expel magma at the Earth's surface. Although less known than magmatic eruptions, gas-driven eruptions expel fragments of preexisting rocks, volcanic gases, and steam, causing substantial casualties. The destructive potential of these eruptions lies in the difficulty in identifying clear warning signals. Some gas-driven eruptions have been preceded by some physicochemical changes, but these were extremely short-term (from minutes to hours), and no long-term trends have been clearly evidenced so far. Here, we show that unheralded gas-driven eruptions can be forecast in the long term using seismic signals recorded at nearby active craters. In particular, we have found that the most recent gas-driven eruptions at Kawah Ijen (Indonesia) and Ruapehu and Tongariro (New Zealand) volcanoes were all preceded by a systematic relative increase in lower-frequency (4.5–8 Hz) seismic amplitude compared to higher frequencies (8–16 Hz) over time scales of months to years. We show that this precursory activity reflects significant increases in seismic attenuation affecting preferentially high-frequency travelling waves; this probably results from the accumulation of volatiles in the shallow crust, which increases pore pressure in small-scale rock heterogeneities and eventually leads to gas-driven eruptions. Our results highlight the feasibility of better constraining the onset and the end of an unrest episode, which is of paramount importance for agencies in charge of volcano monitoring.

INTRODUCTION

Improving the forecasting of small but high-impact gas-driven eruptions is one of the most challenging issues in volcanology and hazards assessment, since several recent catastrophic events have highlighted our limitations to anticipate sudden explosions (e.g., the 2014 Mount Ontake, Japan, volcano eruption; 58 casualties; Yamaoka et al., 2016). Phreatic and hydrothermal eruptions, here grouped under the term gas-driven eruptions, are frequent at three emblematic and hazardous volcanoes: Kawah Ijen (Indonesia) and Ruapehu and Tongariro (New Zealand) (Caudron et al., 2015a; Kilgour et al., 2010). For example, a period of volcanic unrest started at Kawah Ijen in 2011–2012, characterized by a series of sudden gas-driven explosions between 2013 and 2015 during which some of the 200 sulfur miners working daily within the crater lost consciousness (Caudron et al., 2015b, 2018). The last two gas-driven eruptions of Ruapehu volcano occurred in October 2006 and September 2007; the latter seriously injured a climber and caused a lahar that was narrowly avoided by a ski-field groomer (Jolly et al., 2010). A sudden gas-driven eruption also occurred on 6 August 2012 on the northern flank of Tongariro, at the Te Maari vent, after a century of eruptive quiescence in one of the most-visited places in New Zealand (Jolly et al., 2014b). These repeated unforeseen crises severely complicate the decision-making of the agencies monitoring volcanic activity.

A longstanding goal of volcanology is to detect the stress changes occurring around volcanic areas. These stress changes can be detected by monitoring seismic attenuation with local earthquakes (Fehler et al., 1988), although its value as a precursory signal of gas-driven events remains limited by the low number of earthquakes occurring prior to an explosion. Rather than using earthquakes, here we investigate changes in the persistent shallow seismic vibrations by adopting a simple band-ratio approach, named Displacement Seismic Amplitude Ratio (DSAR).

METHOD

Persistent seismic vibrations, often termed volcanic tremor (Konstantinou and Schlindwein, 2003), typically appear at volcanoes experiencing unrest and eruptions. Despite the particular value of volcanic tremor for eruption forecasting (Chouet, 1996; Jellinek and Bercovici, 2011) and monitoring (Fee et al., 2017), no long-term (months) precursory tremor fingerprint has been discovered yet for gas-driven eruptions. This is addressed here by studying the continuous seismic signal recorded at Kawah Ijen, Ruapehu, and Tongariro volcanoes. In particular, we analyze the seismic displacement amplitude evolution between two frequency bands: 4.5–8 Hz (low-frequency in this study) and 8–16 Hz (high-frequency in this study) (see methods in the GSA Data Repository[1]). Both frequency bands were selected to focus on scattering attenuation, which dominates the wavefield >3 Hz (Del Pezzo, 2008). Note that the low-frequency band allows us to minimize the influence of oceanic microseism (<2 Hz; Mordret et al., 2010) and the possible fluctuations of the tremor dominant frequency (<4.5 Hz at the

[1]GSA Data Repository item 2019226, Figure DR1 (DSAR results at Ruapehu based on the lower frequency band used), Figure DR2 (comparison between DSAR and lake temperatures time series at Kawah Ijen), Figure DR3 (DSAR results at Ruapehu and Kawah Ijen based on different days for the moving windows), Figure DR4 (difference between computed DSAR when the instrument response is removed), and Table DR1 (reduced displacements calculated for each volcano), is available online at http://www.geosociety.org/datarepository/2019/, or on request from editing@geosociety.org.

CITATION: Caudron, C., et al., 2019, Change in seismic attenuation as a long-term precursor of gas-driven eruptions: Geology, v. 47, p. 632–636, https://doi.org/10.1130/G46107.1

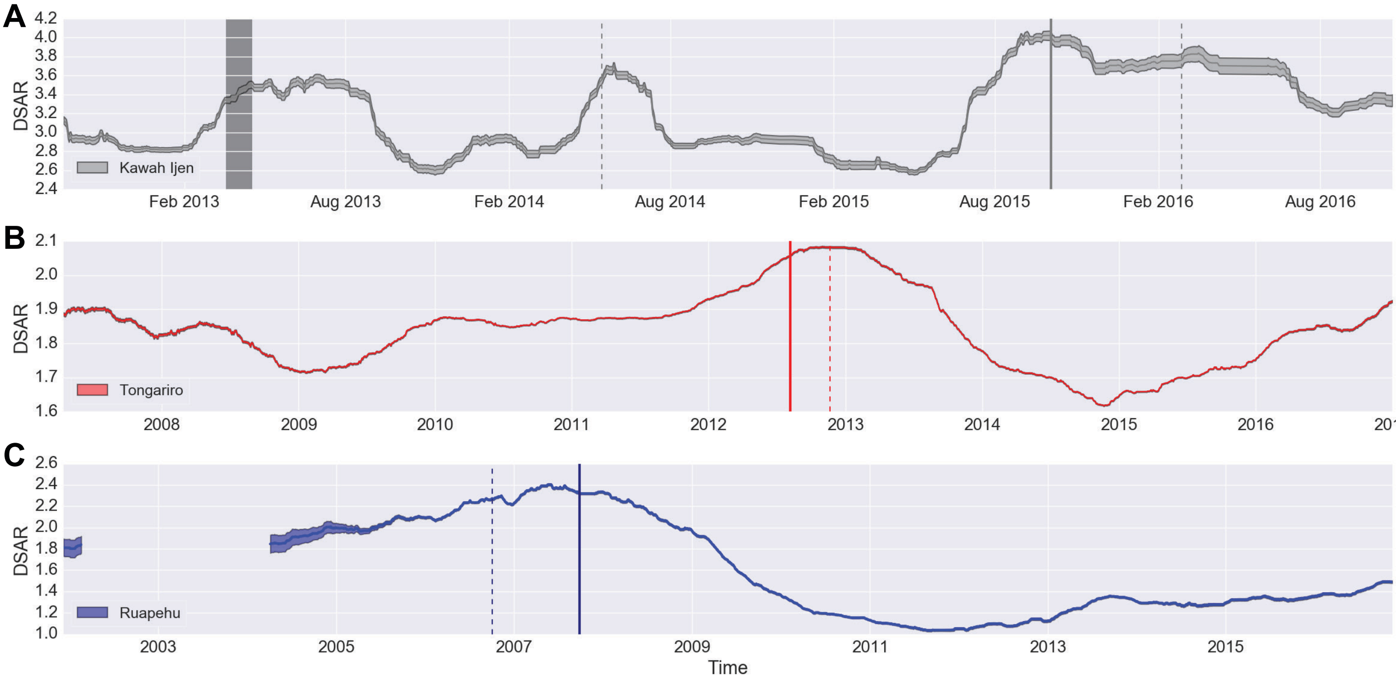

Figure 1. Temporal evolution of Displacement Seismic Amplitude Ratio (DSAR) (see the Data Repository [see footnote 1]) at different volcanoes. A: Kawah Ijen volcano, Indonesia (station POS, on the north crater rim). B: Tongariro volcano, New Zealand (station KRVZ, 2.5 km from the vent). C: Ruapehu volcano, New Zealand (station DRZ, ~100 m from the vent). Small- and large-scale gas-driven explosions are shown as dashed and solid vertical lines, respectively. When eruption lasted for more than 1 day, we used rectangles rather than lines, where width corresponds to duration. Rolling medians of 2 yr were used to smooth 1 d results for Ruapehu and Tongariro, whereas only 90 d was used for shorter time series of Kawah Ijen. Errors for DSAR estimates are represented by the width of the data lines (large width = high errors, small width = low errors). Values for 95% confidence interval (shaded zone) were computed using a bootstrap procedure with 1000 random samples.

target volcanoes), whereas the high-frequency band allows us to be sensitive to small-scale crustal changes due to the shorter wavelength. The use of slightly different bands for the low and high frequencies does not alter our main results, except when we use lower band-spanning frequencies ≤2 Hz (0.5–8 Hz and 2–8 Hz; Fig. DR1 in the Data Repository). After detrending and high-pass filtering the data above 0.5 Hz to avoid the oceanic contamination, the daily signals are filtered in the two frequency bands, and then sliced into 10-min segments. The absolute amplitudes are computed and the ratio between low and high frequencies then exported. The median is computed every day, along with its uncertainty, using a bootstrap procedure with 1000 random samples.

RESULTS

Each small (dashed lines in Fig. 1) and large (solid lines) gas-driven eruption at the three volcanoes occurred when DSAR reached the highest values, after long-term increases (months to years; Fig. 1). At Kawah Ijen, DSAR typically varied in the ~2.60–3.00 range, while gas-driven eruptions (dashed and solid gray lines) were all preceded by DSAR values rising from ~3.00 to at least ~3.60 (Fig. 1A). Values as large as 4.00 ± 0.05 preceded the large explosion in 2015. At Tongariro volcano, DSAR was below ~1.90 between 2007 and 2012, while it steadily increased to 2.10 ± 0.01 prior to the 2012 gas-driven events. After these events, DSAR decreased continuously to 1.60 ± 0.10 in December 2014. Since then, DSAR has been steadily increasing (Fig. 1B). At Ruapehu, DSAR steadily increased from 1.80 ± 0.03 to 2.20 ± 0.02 between 2001 and the small gas-driven eruption in October 2006 (Christenson et al., 2010), reached values of up to 2.40 ± 0.05 (Fig. 1C) prior to the 2007 gas-driven eruption, then decreased and has remained ~1.00–1.50. Importantly, the temporal evolutions of DSAR were more marked at the seismic stations installed nearby the volcano summits (distances <1 km; Fig. 2), probably due to geometric spreading (McNutt, 1992). At 3 km from the summit of the Ngauruhoe volcano (near Tongariro), Jolly et al. (2010) and Park et al. (2019) observed that high frequencies were already muted compared to a station located closer to the summit.

It is worth highlighting that no temporal correlation was observed between DSAR and other observables (Fig. 3). In particular, DSAR trends were not modulated by large regional earthquakes or nearby swarms (Fig. 3A; see the Data Repository), and no correlation exists with the level of volcano seismicity (seismic amplitude filtered between 0.5 and 15 Hz; Fig. 3B), oceanic wave activity (seismic signal filtered between 0.1 and 0.4 Hz at a broadband sensor located near the coast [NZ.KHZ in New Zealand, GE.JAGI in Indonesia; Fig. 3B]), or tidal cycles (Girona et al., 2018). Potential forcing by atmospheric pressure or rainfall were also examined but did not show any consistent correlation with DSAR evolution (Fig. 3C). A potential link with strain was also considered, but GPS data around Tongariro and Ruapehu do not correlate with DSAR time series (Fig. 3D), while no GPS data were available at Kawah Ijen. Interestingly, DSAR peaked at Kawah Ijen when the lake temperature was the highest (Fig. DR2), thus sug-

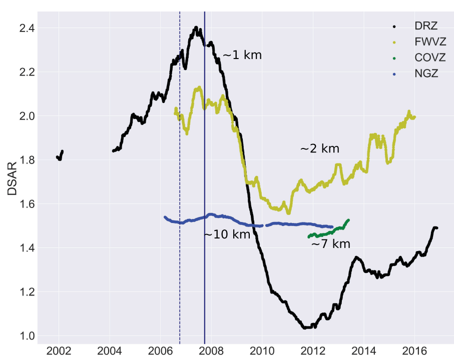

Figure 2. Displacement Seismic Amplitude Ratio (DSAR) (see the Data Repository [see footnote 1]) results at Ruapehu volcano, New Zealand, depending on source-station distance. Seismic station DRZ is on top of the crater; stations FWVZ, COVZ, and NGZ are ~2, 7, and 10 km from the active crater, respectively. Small- and large-scale gas-driven explosions are shown as dashed and solid vertical lines, respectively. Rolling median of 2 yr is used, as in Figure 1.

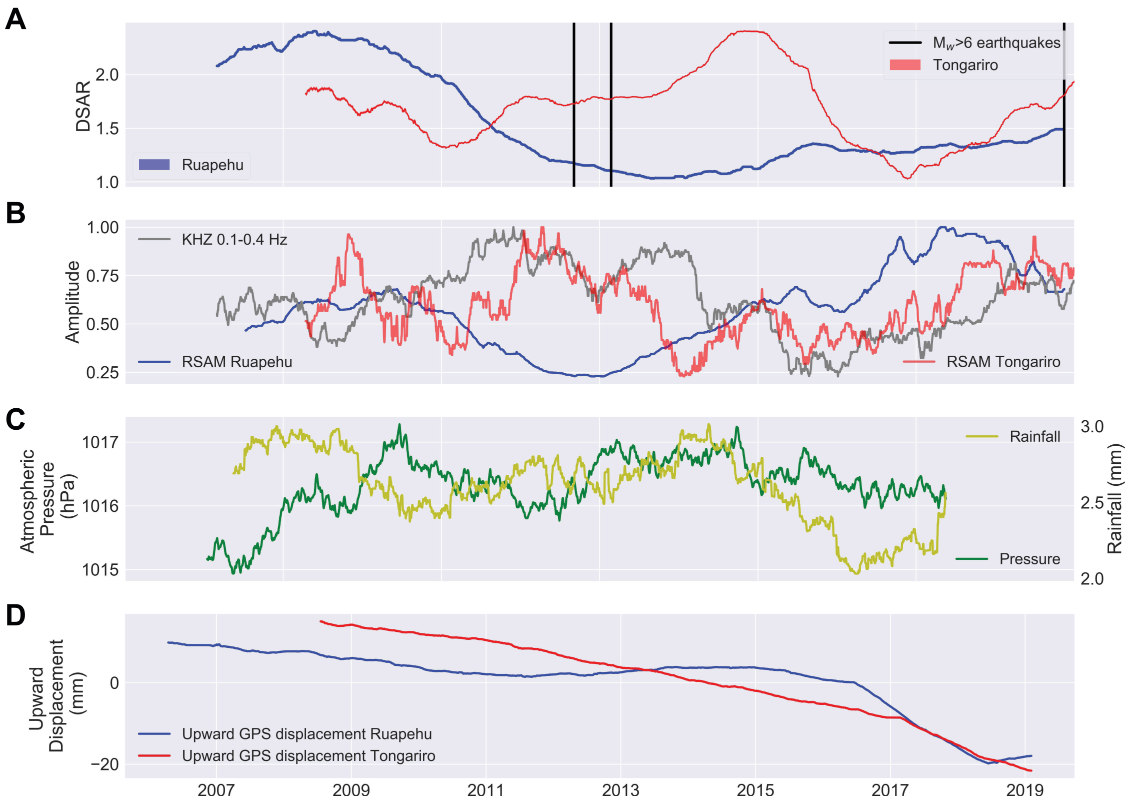

Figure 3. Displacement Seismic Amplitude Ratio (DSAR) (see the Data Repository [see footnote 1]), volcano activity, and external modulators at the studied volcanoes. A: DSAR results at Ruapehu and Tongariro volcanoes, New Zealand. B: Seismic amplitude between 0.5 and 15 Hz at Ruapehu (real-time seismic amplitude measurement [RSAM Ruapehu]; Endo and Murray, 1991) and Tongariro (RSAM Tongariro), and seismic amplitude between 0.1 and 0.4 Hz at a broadband seismometer located near the east coast of the South Island of New Zealand (station KHZ), a proxy for oceanic activity (all normalized to amplitude). C: Rainfall and atmospheric pressure measured on the North Island of New Zealand. D: Upward displacements recorded by GPS stations at Ruapehu (station VGWF) and Tongariro (station VGOT). All data are smoothed using a rolling median of 2 yr.

gesting enhanced heat flux (Lewicki et al., 2016; Caudron et al., 2017b). Therefore, we conclude that DSAR trends were driven primarily by volcanic activity.

MODEL

Our results call for a model to unveil the link between the variations of DSAR, the mechanism that generates the continuous shallow seismicity recorded around the crater of active volcanoes, and the processes that eventually lead to gas-driven eruptions. Based on a recent mechanistic model developed by Girona et al. (2019), we propose that tremor originates in gas cavities trapped beneath active craters (in the so-called steam zone; Hurst and Sherburn, 1993; Christenson et al., 2010) as the result of three concurrent processes (Fig. 4A): (1) the permeable flow of gases through the shallow volcanic edifice; (2) the temporary accumulation of gases in the cavity; and (3) the random supply of magmatic or hydrothermal volatiles to the cavity (e.g., via bubble bursting, channeling in highly viscous magmas, or shear fractures near the conduit walls). Moreover, it is natural to assume that before gas-driven eruptions, volcanic and/or hydrothermal gases also accumulate in the upper layers of the volcanic edifice (i.e., between the gas cavity and the seismic station receiver) (Fig. 4B), thus dramatically increasing pore pressure in the shallow crust and the frequency-dependent attenuation (i.e., scattering attenuation) of the seismic waves that propagate from the source to the receiver (Winkler and Nur, 1979; Jolly et al., 2012; Tsai et al., 2012; Girona et al., 2019; Park et al., 2019). Using the aforementioned approaches, we generated a set of ~13,500 synthetic seismic signals to explore how DSAR varies with increasing

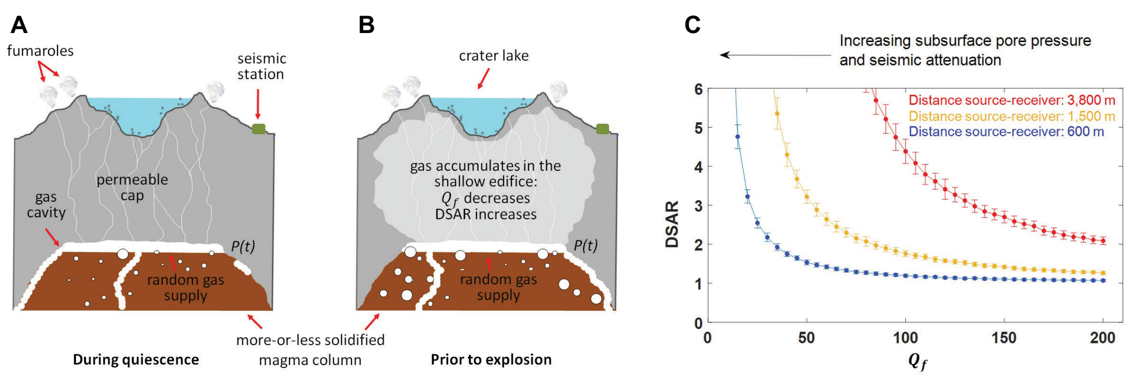

Figure 4. Model for Displacement Seismic Amplitude Ratio (DSAR) (see the Data Repository [see footnote 1]) evolution. A: Sketch of model during quiescence. Tremor-like pressure oscillations *P*(*t*) emerge in gas cavities trapped beneath active degassing craters due to permeable flow of gas through the shallow cap, temporary accumulation of gas in the cavity, and the random supply of gas from depth (e.g., via bubble bursting, bubble connection forming channels, shear fracture close to conduit walls). These pressure oscillations generate seismic waves that propagate from the source to the seismic station (see details in Girona et al., 2019). B: Sketch of model shortly before explosion. Note that gas is expected to accumulate in the shallow volcanic edifice, thus increasing pore pressure, increasing seismic attenuation in the crust, and decreasing the dimensionless quality factor, Q_f. C: Variation of modeled DSAR with Q_f (error bars are standard deviation). We use realistic values for the parameters of the model (see details in the Data Repository); these values allow generating synthetic seismicity with dominant frequencies below ~4.5 Hz, as observed in Ruapehu (New Zealand), Kawah Ijen (Indonesia), and Tongariro (New Zealand) volcanoes.

seismic attenuation (see the Data Repository); increasing seismic attenuation is taken into account by decreasing the seismic quality factor Q_f (Fehler et al., 1988). Our analysis reveals that DSAR systematically increases with decreasing quality factor Q_f and thus with increasing pore pressure below volcanic craters; however, this increase is significant only when Q_f is below a critical threshold that depends on the source-receiver distance (Fig. 4B). For example, for a source-receiver distance on the order of ~600 m (as for Ruapehu and Kawah-Ijen volcanoes), we find that DSAR lies in the range ~1–1.2 for $Q_f > 100$, is increased significantly for $Q_f < 100$, and reaches values of up to 3.23 ± 0.17 as the quality factor decreases to $Q_f = 20$.

DISCUSSION

The increase in DSAR prior to gas-driven eruptions is therefore ascribed to increased pore pressure, the dominant attenuation mechanism in the shallow crust (Winkler and Nur, 1979). The interpretation of our results agrees with that of Keats et al. (2011), who attributed seismic anisotropy changes during the 2006–2007 Ruapehu eruptions to an increase in pore fluid pressure in the region, and that of Christenson et al. (2010), who suggested the long-term development of a seal since the 1995–1996 Ruapehu eruptions, and thus the accumulation of gases in the shallow volcanic edifice. At Tongariro, Hamling et al. (2016) documented subsidence after the 2012 eruption, which coincided with decreased DSAR values. Their interpretation relates to a depressurization in the shallow system that would be consistent with a decrease in seismic attenuation and DSAR.

We note that relative variations of DSAR are greater at Kawah Ijen and Ruapehu (~1.5) than at Tongariro (~0.4). A possible interpretation is that seismic energy losses at Kawah Ijen and Ruapehu are dominated by scattering attenuation, which is strongly frequency dependent (Fehler et al., 1988). When scattering attenuation dominates, commonly the case at volcanoes (Prudencio et al., 2015, 2017a, 2017b), the ratio of low-frequency to high-frequency seismic amplitude is expected to be larger. In turn, enhanced scattering attenuation at 8–16 Hz compared to 4.5–8 Hz could be attributed to the formation of small-scale crustal heterogeneities (Fehler et al., 1988), where volatiles would tend to accumulate prior to explosions. In particular, for surface waves at frequencies ranging between 8 and 16 Hz, the scattering attenuation preferentially affects wavelengths (λ) from 25 m to 70 m ($\lambda = 0.92 \times V_c/f$, where V_c is phase velocity [see the Data Repository] and f is frequency), consistent with the dimensions of newly formed hydrothermal seals (Christenson et al., 2017). The formation of these seals favors the accumulation of gas in the crust and thus an increase in pore pressure, which may eventually lead to gas-driven eruptions. Scattering attenuation would have been only minor at Tongariro, pointing towards a bottom-up trigger due to the influx of gas from a magma reservoir, as previously suggested by Jolly et al. (2014), rather than the formation of a small-scale seal.

To date, only a few studies have investigated temporal changes in seismic attenuation due to the scarcity of repetitive earthquakes. At Ruapehu, Titzschkau et al. (2010) detected a high attenuation anomaly using local earthquakes associated with the 1995–1996 gas-driven eruption, which was ascribed to changes in scattering caused by cracks and pore space. At Mount St. Helens (Washington, USA), however, Fehler et al. (1988) only found a weak frequency dependence on seismic attenuation, presumably due to the dominance of intrinsic attenuation prior to the 1980 eruption. Future studies should shed some light on the relative importance of intrinsic compared to scattering attenuation, and possibly other processes.

The crux of the DSAR methodology relies on a persistent radiation of seismic energy travelling from the source to the seismic instruments. To compare the seismic energy explored in this study with persistent seismic signals recorded at other volcanoes, we have computed the reduced displacement values following McNutt (1992). Overall, the reduced displacements at our studied volcanoes (see the Data Repository, Table DR1) are at least one order of magnitude higher than those of the smallest volcano-hydrothermal tremor recorded elsewhere (Benoit et al., 2003). These results are therefore consistent with a volcano-hydrothermal origin for the persistent seismicity recorded at Kawah Ijen, Ruapehu, and Tongariro, and confirm that the source of seismic waves was strong enough to efficiently sample the shallow volcanic edifice.

In this study, we interpret time-varying DSAR values in terms of seismic attenuation using our model for persistent gas-induced seismicity. At volcanoes lacking a persistent source of seismicity, DSAR can't be interpreted as change in seismic attenuation using our model. Source effects should also be considered, in particular when multiple seismic sources act at the same time at different locations or a single source persistently radiates energy >4.5 Hz. In such cases, DSAR, as a monitoring tool, could reflect a change in the system other than attenuation that would be worth investigating with complementary monitoring and/or modeling tools.

CONCLUSION

Temporal variations in seismic attenuation have been quantified at some volcanoes by using earthquakes, although this methodology prevents the real-time forecasting of gas-driven eruptions in the absence of earthquakes. Our approach overcomes this problem through the use of continuous tremor and may open new doors for volcano monitoring. The objective of the DSAR methodology is not to predict gas-driven eruptions at the day scale, but to provide a long-term forecasting by detecting when volcanoes are in a critical state. Numerous increases in alert levels in the target volcanoes have not been followed by gas-driven eruptions while DSAR values were low, whereas many of the gas-driven eruptions have taken place when the alert level was low but DSAR elevated; this strongly supports the use of our methodology to better assess alert levels in the future. The DSAR technique can also be used to detect the end of an unrest period, which is likewise crucial for monitoring agencies, is remarkably simple, and can be easily implemented in any real-time monitoring scheme—the only requirement being the presence of a seismic station near a volcano summit. Although multiple seismic sources, seismic energy with frequency >4.5 Hz, or the lack of seismic tremor prevent the direct interpretation of DSAR variations as seismic attenuation, the temporal evolution of DSAR variations generally reflects a change in the system, which is valuable for monitoring purposes, as for example in the widely used real-time seismic amplitude measurement (RSAM) approach (Endo and Murray, 1991).

ACKNOWLEDGMENTS

C. Caudron benefited from a Fondation Wiener Anspach postdoctoral fellowship, then from a FNRS Chargé de Recherche postdoctoral grant. T. Girona is currently supported by an appointment to the NASA Postdoctoral Program at the Jet Propulsion Laboratory, California Institute of Technology, administered by Universities Space Research Association under contract with NASA. F. Costa and C. Newhall are acknowledged for fruitful discussion at the initial stages of this idea. We thank N. Fournier, A. Jolly, and B. Christenson for providing critical comments and the list of external modulators at Ruapehu and Tongariro volcanoes. The U.S. Geological Survey Volcano Disaster Assistance Program team, V. van Hinsberg, and A. Bernard helped in the identification and interpretation of gas-driven events at Kawah Ijen. This work comprises Earth Observatory of Singapore contribution 242. This research is partly supported by the National Research Foundation Singapore and the Singapore Ministry of Education under the Research Centres of Excellence initiative. We would like to thank editor Mark Quigley, and Art Jolly, John Pallister, and the anonymous reviewers for their constructive and stimulating suggestions.

REFERENCES CITED

Benoit, J.P., McNutt, S.R., and Barboza, V., 2003, Duration-amplitude distribution of volcanic tremor: Journal of Geophysical Research, v. 108, 2146, https://doi.org/10.1029/2001JB001520.

Caudron, C., Syahbana, D.K., Lecocq, T., Van Hinsberg, V., McCausland, W., Triantafyllou, A., Camelbeeck, T., Bernard, A., and Surono, 2015a, Kawah Ijen volcanic activity: A review: Bulletin of Volcanology, v. 77, 16, https://doi.org/10.1007/s00445-014-0885-8.

Caudron, C., Lecocq, T., Syahbana, D.K., McCausland, W., Watlet, A., Camelbeeck, T., Bernard, A., and Surono, 2015b, Stress and mass changes at a wet volcano: Example during the 2011–2012

volcanic unrest at Kawah Ijen volcano (Indonesia): Journal of Geophysical Research: Solid Earth, v. 120, p. 5117–5134, https://doi.org/10.1002/2014JB011590.
Caudron, C., Campion, R., Rouwet, D., Lecocq, T., Capaccioni, B., Syahbana, D., Suparjan, Purwanto, B.H., and Bernard, A., 2017a, Stratification at the Earth's largest hyperacidic lake and its consequences: Earth and Planetary Science Letters, v. 459, p. 28–35, https://doi.org/10.1016/j.epsl.2016.11.002.
Caudron, C., Mauri, G., Williams-Jones, G., Lecocq, T., Syahbana, D.K., De Plaen, R., Peiffer, L., Bernard, A., and Saracco, G., 2017b, New insights into the Kawah Ijen hydrothermal system from geophysical data, *in* Ohba, T., et al., eds., Geochemistry and Geophysics of Active Volcanic Lakes: Geological Society of London Special Publication 437, p. 57–72, https://doi.org/10.1144/SP437.4.
Caudron, C., Taisne, B., Neuberg, J., Jolly, A.D., Christenson, B., Lecocq, T., Suparjan, Syahbana, D., and Suantika, G., 2018, Anatomy of phreatic eruptions: Earth, Planets, and Space, v. 70, 168, https://doi.org/10.1186/s40623-018-0938-x.
Chouet, B.A., 1996, Long-period volcano seismicity: Its source and use in eruption forecasting: Nature, v. 380, p. 309–316, https://doi.org/10.1038/380309a0.
Christenson, B.W., Reyes, A.G., Young, R., Moebis, A., Sherburn, S., Cole-Baker, J., and Britten, K., 2010, Cyclic processes and factors leading to phreatic eruption events: Insights from the 25 September 2007 eruption through Ruapehu crater lake, New Zealand: Journal of Volcanology and Geothermal Research, v. 191, p. 15–32, https://doi.org/10.1016/j.jvolgeores.2010.01.008.
Christenson, B.W., White, S., Britten, K. and Scott, B.J., 2017, Hydrological evolution and chemical structure of a hyper-acidic spring-lake system on Whakaari/White Island, NZ: Journal of Volcanology and Geothermal Research, v. 346, p.180–211, https://doi.org/10.1016/j.jvolgeores.2017.06.017.
Del Pezzo, E., 2008, Seismic wave scattering in volcanoes: Advances in Geophysics, v. 50, p. 353–371, https://doi.org/10.1016/S0065-2687(08)00013-7.
Endo, E.T., and Murray, T., 1991, Real-time seismic amplitude measurement (RSAM): A volcano monitoring and prediction tool: Bulletin of Volcanology, v. 53, p. 533–545, https://doi.org/10.1007/BF00298154.
Fee, D., Haney, M.M., Matoza, R.S., Eaton, A.R., Cervelli, P., Schneider, D.J., and Iezzi, A.M., 2017, Volcanic tremor and plume height hysteresis from Pavlof volcano, Alaska: Science, v. 355, p. 45–48, https://doi.org/10.1126/science.aah6108.
Fehler, M., Roberts, P., and Fairbanks, T., 1988, A temporal change in coda wave attenuation observed during an eruption of Mount St. Helens: Journal of Geophysical Research, v. 93, p. 4367–4373, https://doi.org/10.1029/JB093iB05p04367.
Girona, T., Huber, C., and Caudron, C., 2018, Sensitivity to lunar cycles prior to the 2007 eruption of Ruapehu volcano: Scientific Reports, v. 8, 1476, https://doi.org/10.1038/s41598-018-19307-z.
Girona, T., Caudron, C., and Huber, C., 2019, Origin of shallow volcanic tremor: the dynamics of gas pockets trapped beneath thin permeable media: Journal of Geophysical Research: Solid Earth, https://doi.org/10.1029/2019JB017482.
Hamling, I.J., Williams, C.A., and Hreinsdóttir, S., 2016, Depressurization of a hydrothermal system following the August and November 2012 Te Maari eruptions of Tongariro, New Zealand: Geophysical Research Letters, v. 43, p. 168–175, https://doi.org/10.1002/2015GL067264.
Hurst, A.W., and Sherburn, S., 1993, Volcanic tremor at Ruapehu: Characteristics and implications for the resonant source: New Zealand Journal of Geology and Geophysics, v. 36, p. 475–485, https://doi.org/10.1080/00288306.1993.9514593.
Jellinek, A.M., and Bercovici, D., 2011, Seismic tremors and magma wagging during explosive volcanism: Nature, v. 470, p. 522–525, https://doi.org/10.1038/nature09828.
Jolly, A.D., Sherburn, S., Jousset, P., and Kilgour, G., 2010, Eruption source processes derived from seismic and acoustic observations of the 25 September 2007 Ruapehu eruption—North Island, New Zealand: Journal of Volcanology and Geothermal Research, v. 191, p. 33–45, https://doi.org/10.1016/j.jvolgeores.2010.01.009.
Jolly, A.D., Jousset, P., Lyons, J.J., Carniel, R., Fournier, N., Fry, B., and Miller, C., 2014a, Seismo-acoustic evidence for an avalanche driven phreatic eruption through a beheaded hydrothermal system: An example from the 2012 Tongariro eruption: Journal of Volcanology and Geothermal Research, v. 286, p. 331–347, https://doi.org/10.1016/j.jvolgeores.2014.04.007.
Jolly, G.E., Keys, H.J.R., Procter, J.N., and Deligne, N.I., 2014b, Overview of the co-ordinated risk-based approach to science and management response and recovery for the 2012 eruptions of Tongariro volcano, New Zealand: Journal of Volcanology and Geothermal Research, v. 286, p. 184–207, https://doi.org/10.1016/j.jvolgeores.2014.08.028.
Keats, B.S., Johnson, J.H., and Savage, M.K., 2011, The Erua earthquake cluster and seismic anisotropy in the Ruapehu region, New Zealand: Geophysical Research Letters, v. 38, L16315, https://doi.org/10.1029/2011GL049014.
Kilgour, G., Manville, V., Della Pasqua, F., Graettinger, A., Hodgson, K.A., and Jolly, G.E., 2010, The 25 September 2007 eruption of Mount Ruapehu, New Zealand: Directed ballistics, surtseyan jets, and ice-slurry lahars: Journal of Volcanology and Geothermal Research, v. 191, p. 1–14, https://doi.org/10.1016/j.jvolgeores.2009.10.015.
Konstantinou, K.I., and Schlindwein, V., 2003, Nature, wavefield properties and source mechanism of volcanic tremor: A review: Journal of Volcanology and Geothermal Research, v. 119, p. 161–187, https://doi.org/10.1016/S0377-0273(02)00311-6.
Lewicki, J.L., Caudron, C., van Hinsberg, V.J., and Hilley, G.E., 2016, High spatio-temporal resolution observations of crater lake temperatures at Kawah Ijen volcano, East Java, Indonesia: Bulletin of Volcanology, v. 78, 53, https://doi.org/10.1007/s00445-016-1049-9.
McNutt, S.R., 1992, Volcanic tremor, *in* Nierenberg, W.A., ed., Encyclopedia of Earth System Science, volume 4: Academic Press, p. 417–425.
Mordret, A., Jolly, A.D., Duputel, Z., and Fournier, N., 2010, Monitoring of phreatic eruptions using interferometry on retrieved cross-correlation function from ambient seismic noise: Results from Mt. Ruapehu, New Zealand: Journal of Volcanology and Geothermal Research, v. 191, p. 46–59, https://doi.org/10.1016/j.jvolgeores.2010.01.010.
Park, I., Jolly, A., Kim, K.Y., and Kennedy, B., 2019, Temporal variations of repeating low frequency volcanic earthquakes at Ngauruhoe Volcano, New Zealand: Journal of Volcanology and Geothermal Research, v. 373, p. 108–119, https://doi.org/10.1016/j.jvolgeores.2019.01.024.
Prudencio, J., Del Pezzo, E., Ibáñez, J.M., Giampiccolo, E., and Patané, D., 2015, Two-dimensional seismic attenuation images of Stromboli Island using active data: Geophysical Research Letters, v. 42, p. 1717–1724, https://doi.org/10.1002/2015GL063293.
Prudencio, J., Aoki, Y., Takeo, M., Ibáñez, J.M., Del Pezzo, E., and Song, W., 2017a, Separation of scattering and intrinsic attenuation at Asama volcano (Japan): Evidence of high volcanic structural contrasts: Journal of Volcanology and Geothermal Research, v. 333, p. 96–103, https://doi.org/10.1016/j.jvolgeores.2017.01.014.
Prudencio, J., Taira, T., Aoki, Y., Aoyama, H., and Onizawa, S., 2017b, Intrinsic and scattering attenuation images of Usu volcano, Japan: Bulletin of Volcanology, v. 79, 29, https://doi.org/10.1007/s00445-017-1117-9.
Titzschkau, T., Savage, M., and Hurst, T., 2010, Changes in attenuation related to eruptions of Mt. Ruapehu Volcano, New Zealand: Journal of Volcanology and Geothermal Research, v. 190, p. 168–178, https://doi.org/10.1016/j.jvolgeores.2009.07.012.
Tsai, V.C., Minchew, B., Lamb, M.P., and Ampuero, J.-P., 2012, A physical model for seismic noise generation from sediment transport in rivers: Geophysical Research Letters, v. 39, L02404, https://doi.org/10.1029/2011GL050255.
Winkler, K., and Nur, A., 1979, Pore fluids and seismic attenuation in rocks: Geophysical Research Letters, v. 6, p. 1–4, https://doi.org/10.1029/GL006i001p00001.
Yamaoka, K., Geshi, N., Hashimoto, T., Ingebritsen, S.E., and Oikawa, T., 2016, Special issue "The phreatic eruption of Mt. Ontake volcano in 2014": Earth, Planets and Space, v. 68, 175, https://doi.org/10.1186/s40623-016-0548-4.

Printed in USA